Robotica (2019) volume 37, pp. 998–1019. © Cambridge University Press 2019
doi:10.1017/S0263574718001406

A Hybrid Obstacle-Avoidance Method of Spatial Hyper-Redundant Manipulators for Servicing in Confined Space

Zonggao Mu†, Tianliang Liu†, Wenfu Xu†*, Yunjiang Lou†, and Bin Liang‡

†*The School of Mechanical Engineering and Automation, Harbin Institute of Technology, Shenzhen 518055, China*
E-mails: muzonggao@163.com, ltianliang2016@gmail.com, louyj@hit.edu.cn
‡*Department of Automation, School of Information Science and Technology, Tsinghua University, Beijing 100084, China*
E-mail: bliang@mail.tsinghua.edu.cn

(Accepted December 5, 2018. First published online: January 14, 2019)

SUMMARY
Due to a large number of redundant degrees of freedom (DOFs), the hyper-redundant manipulator shows outstanding dexterity and adaptability in avoiding the obstacles in confined space. In this paper, a hybrid obstacle-avoidance method of spatial hyper-redundant manipulators is proposed, with both efficiency and accuracy considered. The space around an obstacle is classified into safe, warning, and dangerous zones. A two-level protection strategy is then addressed to handle the obstacle-avoidance problem from qualitative (i.e., pseudo-distance based on super-quadric function) and quantitative (i.e., Euclidean distance based on practical geometry function) perspectives, respectively. The only condition for switching between the two-level protections is the value of pseudo-distance. Then, a modified modal method, which is a trajectory planning method, is presented to plan the collision-free trajectory of the manipulator by maximizing the minimum pseudo-distance or Euclidean distance in different zones. Some parameters, including the arm-angle parameters and the equivalent link length parameters, are defined to represent the manipulator configuration. They are adjusted to avoid the obstacle, singularity, and joint limit. The simulations of 12-DOF manipulator and an experiment of 18-DOF manipulator verify the proposed methods.

KEYWORDS: Hyper-redundant manipulator; Space manipulator; Obstacle avoidance; Modified modal method; Confined space.

1. Introduction

With the development of science and technology, a variety of complex equipment is emerging gradually, for example, nuclear facilities and spacecraft.[1–4] For the service in confined space, the hyper-redundant manipulator shows better dexterity than the non-redundant manipulator in avoiding obstacles. Obviously, the modeling of obstacles and their avoidance are the two key issues for applications of hyper-redundant manipulators. Traditionally, most obstacle modeling methods have simplified the obstacle model, considering only efficiency or accuracy. In fact, whether for two-dimensional (2-D) modeling or three-dimensional (3-D) modeling, most methods have put more emphasis on efficiency. For 2-D obstacle modeling, basic geometric primitives (i.e., line, circle, and ellipse) are always used to model obstacles. Colbaugh et al.[5] modeled the planar obstacle

* Corresponding author. E-mail: wfxu@hit.edu.cn

https://doi.org/10.1017/S0263574718001406 Published online by Cambridge University Press

and manipulator using circles and straight lines, respectively. This simplified approach satisfied the demand for obstacle-avoidance planning in time-varying environments. Later, Rahmanian-Shahri et al.[6] proposed another online collision detection method using ellipses to model links and obstacles in the plane. Perdereau et al.[7] offered a feasible solution for the real-time operation of a redundant robot moving in a variable environment. The method of formulating anti-collision constraints using a concept of pseudo-distance was realized in a simple and original way. For 3-D obstacle modeling, basic space geometric shapes (i.e., sphere, ellipsoid, cylinder, and cuboid) are frequently applied to model spatial obstacles. Bonner and Kelley[8] put forward the successive spherical approximation scheme for the representation of obstacles, which facilitated rapid collision-free path planning in dynamic environments. Choi and Kim[9] presented a "collidability measure" for redundant manipulators, using the sphere and ellipsoid to model the obstacle and manipulator and defining the collidability measure based on the relative movement between links and obstacles. Hwang et al.[10] simplified the mathematical representation and reduced the computation complexity by modeling the objects as ellipsoids. The intersection check was reduced to test whether the point (representing the robot) fell outside or inside the transformed ellipsoid (representing the obstacle). Patel et al.[11] modeled the arm and its environment using cylinders and spheres. By resorting to the notion of dual angles and dual vectors that represented axes of cylinders in space, different types of collision were characterized. Furthermore, super-quadric used by Khosla[12,13] was a typical way to model the basic space geometric shapes in artificial potentials. Pseudo-distance was prior used to calculate the distance from obstacle. Mu et al.[14,15] developed the pseudo-distance concept by establishing a unified modeling framework for multiple moving obstacles. The obstacle surface was represented by a super-quadric function whose parameters could be adjusted to describe different shapes and dimensions.

Once obstacle modeling is completed, online obstacle avoidance becomes the key issue. Glass et al.[16] represented the online obstacle-avoidance requirements as inequality constraints. They achieved obstacle avoidance by satisfying these inequality constraints, when the end-effector tracked the desired trajectory. Yoshida et al.[17] proposed a general and practical online planning framework for generating 3-D collision-free motions. They obtained a collision-free path through efficient geometric and kinematic sampling-based motion planning. Freund et al.[18] presented an approach for the online planning of collision-free robot motions. This approach resulted in an intuitively comprehensible model used to determine the potential collision and treated collision-free path planning as an optimization problem. This optimization problem provided a mathematically exact solution to the path-planning problem by considering all of the static and dynamic obstacles in the environment. Mayorga[19] proposed a fast and geometrically bounded method of online obstacle avoidance for redundant manipulators. This approach was based on the solution of a linear system. The developed algorithm was successfully tested through simulations of a 7-degree of freedom (DOF) redundant manipulator. Seraji[20] formulated the collision-avoidance problem as a position-based force control problem. This approach was simple, computationally fast, and applicable to the whole-arm collision avoidance for the 7-DOF manipulator. For the singularity analysis and avoidance, the similar concepts of the elementary Jacobian transformation, workspace decomposition, and singularity separation methods[21,22] can be used for such hyper-redundant manipulators. Moreover, as general methods, the Damped Least-Squares, Manipulability Optimization, and the Singular Value Filtering methods proposed by other scholars[23,24] can also be used. Limited by the length of the paper, the details are not given in this paper.

The obstacle modeling and avoidance problems for 7-DOF manipulators have been studied extensively. However, few obstacle modeling and avoidance studies have considered both efficiency and accuracy, especially for spatial hyper-redundant manipulators. When efficiency is the factor of concern in modeling, the actual accurate distance always goes unconsidered. In contrast, if an accurate model is built, the computation load is always large during the working process. For example, the model described by the super-quadric function is an efficient way to detect collision, yet it is not accurate in terms of distance. If a model described by a practical geometry function could also be established to calculate the accurate minimum distance when the actual distance is too close, then the actual available workspace would become larger, and the operation of the manipulator would be more secure. Inspired by this idea and the aforementioned literature, this paper proposes a hybrid modeling method combined with a super-quadric function and a practical geometry function. It also uses the modified modal method for the hyper-redundant manipulator to avoid the obstacles described by the proposed hybrid models. The remainder of this paper is organized as follows. In Section 2, the

https://doi.org/10.1017/S0263574718001406 Published online by Cambridge University Press

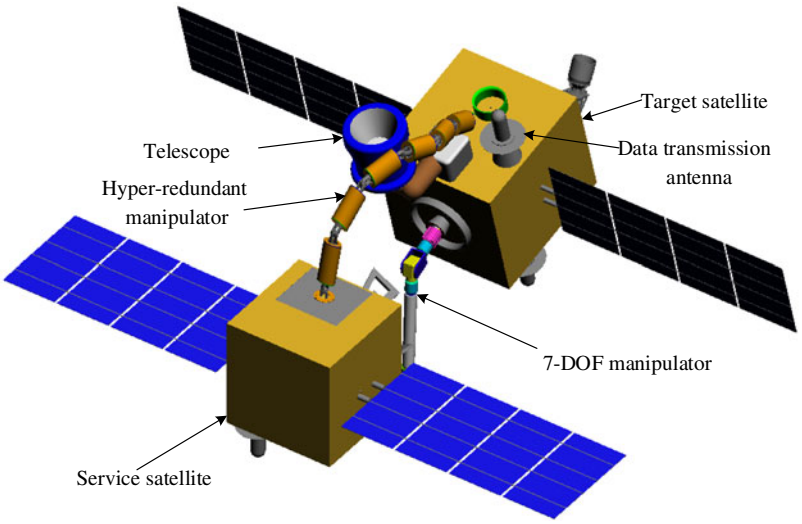


Fig. 1. Hyper-redundant manipulator working in confined space.

hybrid obstacle-avoiding strategies are proposed, and the hybrid obstacle-avoiding concept is established. In Section 3, the mixing qualitative and quantitative criteria are established, and the concrete realization method of the model described by the super-quadric function and the model described by the geometric function are analyzed. In Section 4, obstacle-avoiding trajectory planning using a modified modal function is analyzed. The effectiveness of the proposed algorithm is then verified by simulations and experiment in Section 5. The final section summarizes and concludes the paper.

2. Hybrid Obstacle-Avoiding Strategies

2.1. A hyper-redundant manipulator for on-orbital servicing

Hyper-redundant manipulators play a paramount role in on-orbit servicing applications, especially in narrow environments with multiple obstacles. One typical application scene for satellite maintenance is shown in Fig. 1, where a hyper-redundant manipulator is used to cross the equipment to provide visual information.

The equipment (such as the telescope, optical camera, communication antenna, and attitude sensor) becomes "obstacles" for the working manipulator. To work safely during the whole process, it is necessary to prevent the hyper-redundant manipulator from colliding with space equipment and to prevent the manipulator from being damaged by other obstacles. As such, a hybrid obstacle-avoidance method involving spatial hyper-redundant manipulators for on-orbital servicing is detailed in the following sections.

The hyper-redundant manipulator is connected by universal joints in series. The universal joints have two orthogonal DOFs. This hyper-redundant manipulator is compact in structure and flexible in 3-D motion. These characteristics make it suitable for complex 3-D space tasks. Note that the number of DOFs is n. The odd-numbered $(2i-1)^{\text{th}}$ universal joint is U_{2i-1} and the even-numbered $(2i)^{\text{th}}$ universal joint is U_{2i}, where $i = 1, 2, \ldots, N$ $(N = n/4)$. The Denavit-Hartenberg (D-H) parameters and the D-H coordinate system are shown in Table I and Fig. 2, respectively.

2.2. Hybrid obstacle-avoiding concept

When the hyper-redundant manipulator performs space tasks, obstacles can be avoided in two ways: through the motion of the whole hyper-redundant manipulator[25–27] or through the local adjustment of several related joints. The former way is suitable for relatively spacious environments. However, the latter way is more suitable for making full use of a narrow space with multiple obstacles. This paper focuses on providing a solution to the latter issue. Therefore, all equipment in the task space is modeled according to the value and urgency of avoidance. Based on the idea of the aforementioned hybrid method in Section 1, the hybrid obstacle modeling of the space equipment is established synergistically using the super-quadric and practical geometry functions (as shown in Fig. 3).

https://doi.org/10.1017/S0263574718001406 Published online by Cambridge University Press

Table I. D-H parameter table.

Link i	θ_i (°)	α_i (°)	a_i (m)	d_i (m)
1	0	90	0	0
2	0	0	L	0
3	0	−90	0	0
4	0	0	L	0
...	...	...	...	...
$n-3$	0	90	0	0
$n-2$	0	0	L	0
$n-1$	0	−90	0	0
n	0	0	L	0

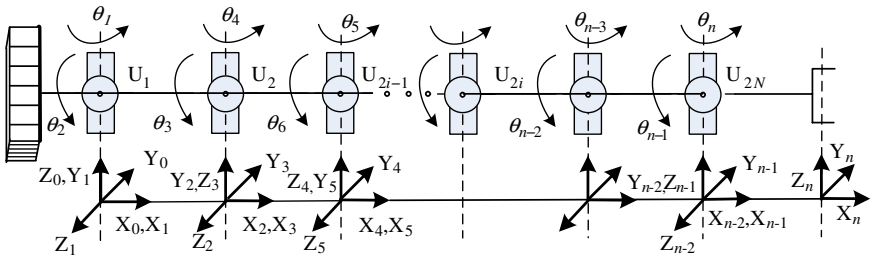


Fig. 2. D-H coordinate system.

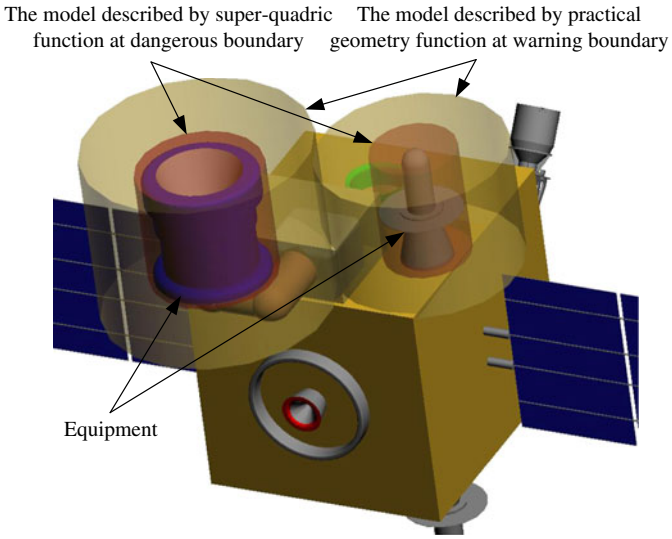


Fig. 3. Hybrid obstacle modeling of the space equipment.

As shown in Figs. 3 and 4, each obstacle is surrounded by two kinds of models. The dimension of the model described using the super-quadric function is much larger than that of the obstacle. However, the dimension of the model described using the practical geometry function is similar to that of the obstacle. For the model described using the super-quadric function, the collision can be determined rapidly according to the pseudo-distance, although this is simply a qualitative detection method. However, the model described using the practical geometry function can not only obtain the Euclidean distance between the manipulator and the obstacle, but also resolve the coordinate of the nearest distance accurately. This geometric model must distinguish the relative position and adopt quite different calculation methods. If the Euclidean distance is calculated during the whole working process, the huge amount of computation is the major adverse effect on real-time obstacle avoidance. Therefore, for the preceding reasons, the model described using the super-quadric function is generally defined at the warning boundary of the obstacle, and the model described using the practical

https://doi.org/10.1017/S0263574718001406 Published online by Cambridge University Press

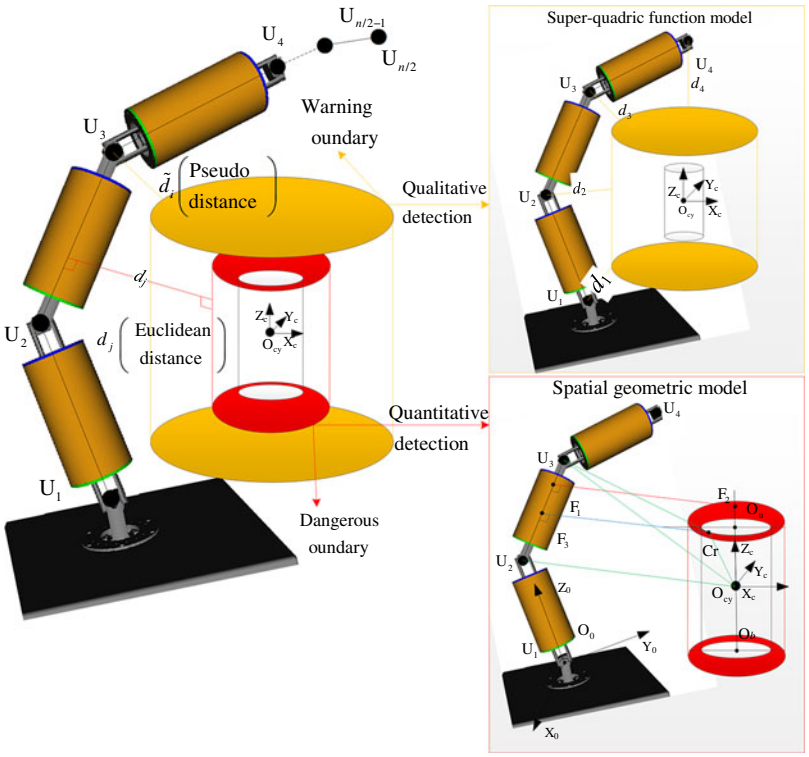


Fig. 4. Detection of pseudo-distance and Euclidean distance.

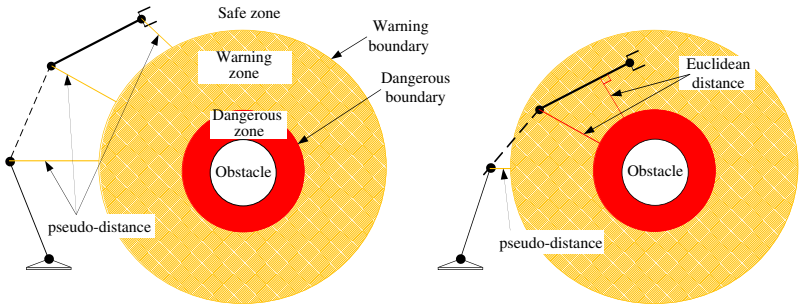


Fig. 5. Relationship between the manipulator and obstacle.

geometry function is defined at the dangerous boundary of the obstacle. The relationship between the manipulator and the obstacle is drawn in Fig. 5. There are three application principles for hybrid models of obstacles and their avoidance.

1) When the manipulator is in the safe zone (i.e., the pseudo-distance is more than zero), the pseudo-distance is calculated efficiently based on the model described using the super-quadric function. The qualitative criterion for the manipulator movement can be provided, and the computation load of the obstacle avoidance is relatively small.
2) When the manipulator is in the warning zone (i.e., the pseudo-distance is no more than zero), the obstacle-avoidance strategy takes account of both security and the computation load. The Euclidean distance is accurately calculated based on the model described using the practical geometry function, and the quantitative criteria can be provided for the obstacle-avoidance planning.
3) When the manipulator is approaching the dangerous boundary, security is the main focus of the obstacle-avoidance strategy. The Euclidean distance based on the model described using the practical geometry function can provide not only the nearest distance, but also the nearest point on the manipulator, and the obstacle can be avoided.

https://doi.org/10.1017/S0263574718001406 Published online by Cambridge University Press

Table II. Obstacle-avoidance strategy criterion.

Zone	Dangerous boundary	Warning zone	Warning boundary	Safe zone
Motion of manipulator	Stop	Slow (Criterion: Euclidean distance)	Deceleration	Normal speed (Criterion: pseudo-distance)

The corresponding obstacle-avoidance strategy criterion is shown in Table II. The corresponding pseudo-distance or Euclidean distance and the corresponding operation speed can be chosen according to the equipment value, threshold criterion, and space-ground time delay.

3. Mixing Qualitative and Quantitative Criteria

The hybrid obstacle-avoidance modeling method consists of the model described using the super-quadric function and the model described using the practical geometry function. The pseudo-distance can be taken as the distance criteria qualitatively, while the Euclidean distance can be taken as the distance criteria quantitatively.

3.1. Qualitative criterion based on the model described using the super-quadric function

As the basic geometric model can represent the obstacle, the super-quadric function is used to establish the mathematical equation of the basic geometric model. The most obvious advantage of this model is that the typical geometric shapes can be modeled in the unified formula. The representation of any point P(x, y, z) on a super-quadric function is listed in unified Eq. (1). The relationship between spatial points and the model described using the super-quadric function is shown in Fig. 6.

$$^{\mathrm{b}}S(x, y, z) = \left(\frac{(x - x_0)}{h_1}\right)^{2m} + \left(\frac{(y - y_0)}{h_2}\right)^{2n} + \left(\frac{(z - z_0)}{h_3}\right)^{2p} - 1 = 0 \tag{1}$$

The left superscript "b" indicates the obstacle's fixed coordinate system. The size of the basic geometric model is represented by h_1, h_2, and h_3. The type of the basic geometry model (sphere, cylinder, cuboid or cone, etc.) is indicated by $m \geq 1$, $n \geq 1$, and $p \geq 1$. The location of the obstacle geometry center in its own coordinate system {b} is indicated by x_0, y_0, and z_0. By adjusting the parameters of the super-quadric function, the shapes of different basic geometries can be expressed, which is detailed in our previous study.[15]

Relative to the obstacle (the cylinder is taken as the example in this paper), the points in space can be divided into three categories (shown in Fig. 6): 1) the points inside the obstacle (collision), 2) the points on the obstacle surface (critical position of collision), and 3) the points outside the obstacle (no collision).

$$S(x, y, z) = (x)^2 + (y)^2 + (z)^8 - 1 \tag{2}$$

When the points are changing along the lines $\left(\text{i.e., } l_{1:}\begin{cases} x = v \\ y = 0 \\ z = 0 \end{cases}, l_{2:}\begin{cases} x = 0 \\ y = 0 \\ z = v \end{cases}, l_{3:}\begin{cases} x = v \\ y = v \\ z = v \end{cases}, l_{4:}\begin{cases} x = v \\ y = v \\ z = 2v \end{cases}\right)$ in Fig. 6, the relationship of the pseudo-distance between the spatial points and the cylindrical obstacle is shown in Fig. 7. The variable and the pseudo-distance are abbreviated as v and pd, respectively.

For the cylindrical obstacle model, the approaching direction and the change rate of the pseudo-distance are listed in Table III.

The change rate of the pseudo-distance is quite different along the corresponding lines. For the different approach directions, the unified criteria of the distance between the manipulator and the obstacle are difficult to set based on the pseudo-distance of the model described by the super-quadric function. However, the collision can be found easily and quickly by comparing the relationship between the value of $S(x_{\mathrm{p}}, y_{\mathrm{p}}, z_{\mathrm{p}})$ and 0 (the relationship is shown in Fig. 6). As such, the model described using the super-quadric function can be built much larger than the actual obstacle, and it is also defined as the warning boundary. The computation load of the qualitative criterion is small, and the efficiency of the qualitative criterion is ensured.

https://doi.org/10.1017/S0263574718001406 Published online by Cambridge University Press

Table III. Approaching direction and change rate of pseudo-distance.

Approaching direction	**Changing rate of pseudo-distance**
l_1	$\left.\frac{\partial S(x,y,z)}{\partial x}\right\|_{x=v} = 2v$
l_2	$\left.\frac{\partial S(x,y,z)}{\partial z}\right\|_{z=v} = 8v^7$
l_3	$\left.\frac{\partial S(x,y,z)}{x} + \frac{\partial S(x,y,z)}{y} + \frac{\partial S(x,y,z)}{z}\right\|_{x=y=z=v} = 4v + 8v^7$
l_4	$\left.\frac{\partial S(x,y,z)}{x} + \frac{\partial S(x,y,z)}{y} + \frac{\partial S(x,y,z)}{z}\right\|_{x=y=v,z=2v} = 4v + 1024v^7$

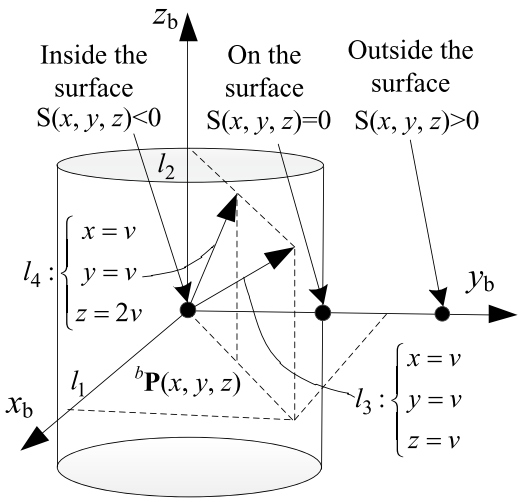


Fig. 6. Relationship between spatial points and the model described using the super-quadric function.

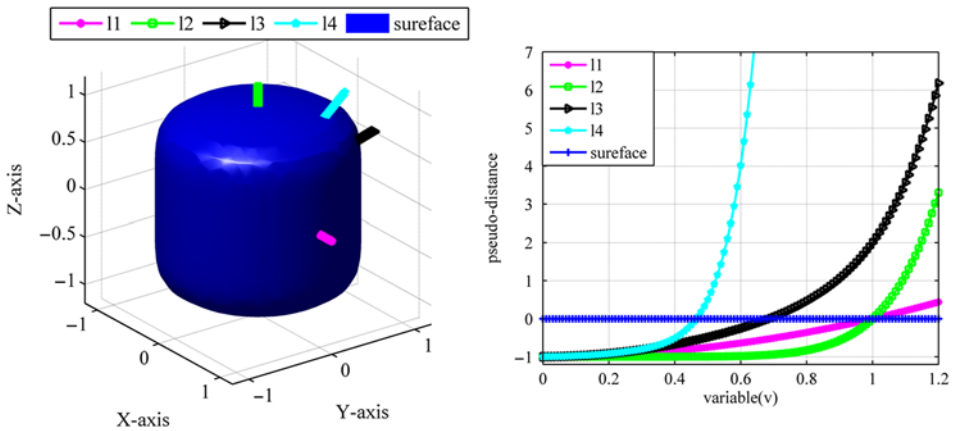


Fig. 7. Approaching direction to cylinder (left) and the corresponding pseudo-distance (right).

3.2. Quantitative criterion based on the model described using the practical geometry function

Analysis of the model described using the practical geometry function reveals that the minimum distance between the manipulator and the obstacle mainly appears in three cases: 1) the perpendicular distance 1, which is between the obstacle and the link; 2) the perpendicular distance 2, which is between the upper or bottom surfaces of the obstacle and the link; and 3) the perpendicular distance 3, which is between the upper or bottom surfaces of the link and the obstacle. In this paper, the three typical calculation processes of the perpendicular distances are discussed. To facilitate the expression,

https://doi.org/10.1017/S0263574718001406 Published online by Cambridge University Press

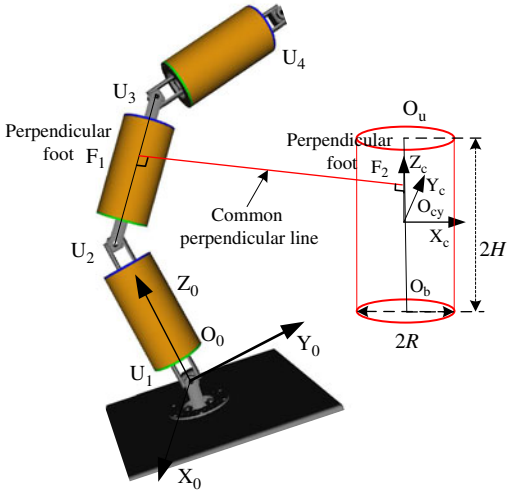


Fig. 8. Two perpendicular feet located on the manipulator and obstacle, respectively.

the coordinates of the base and each link are transformed into the coordinate system of the obstacle. In this section, only the cylindrical obstacle is taken as an example.

(1) Perpendicular distance 1

The perpendicular line is the shortest distance between the two spatial segments. When two perpendicular feet (i.e., F_1 and F_2) are located on the manipulator and the obstacle, respectively, the minimum distance between the link and the obstacle is the length of the common perpendicular line F_1F_2, which is shown in Fig. 8.

The geometrical equation of the cylinder is as follows:

$$\begin{cases} \left(x - x_{O_{cy}}\right)^2 + \left(y - y_{O_{cy}}\right)^2 = R^2 \\ -H \le z \le H \end{cases} \tag{3}$$

where the center of the obstacle is $P_{O_{cy}}\left(x_{O_{cy}}, y_{O_{cy}}, z_{O_{cy}}\right)$, the radius is R, the height is $2H$, the center of the upper surface is O_u, the center of the bottom surface is O_b, the direction vector is $\overrightarrow{O_bO_u} = [0, 0, 1]$, and the direction vector of the link is $\overrightarrow{U_2U_3} = \left[x_{U_3} - x_{U_2}, y_{U_3} - y_{U_2}, z_{U_3} - z_{U_2}\right]$.

The perpendicular foot of the perpendicular line is F_i. The perpendicular equation F_1F_2 is shown in Fig. 8:

$$\frac{x - x_{F_1}}{x_{F_2} - x_{F_1}} = \frac{y - y_{F_1}}{y_{F_2} - y_{F_1}} = \frac{z - z_{F_1}}{z_{F_2} - z_{F_1}}. \tag{4}$$

The direction vector is $\overrightarrow{F_1F_2} = \left[x_{F_2} - x_{F_1}, y_{F_2} - y_{F_1}, z_{F_2} - z_{F_1}\right]$.

According to the geometric properties of the perpendicular foot:

$$\begin{cases} \overrightarrow{F_1F_2} \cdot \overrightarrow{O_bO_u} = 0 \\ \overrightarrow{F_1F_2} \cdot \overrightarrow{U_2U_3} = 0 \end{cases}. \tag{5}$$

Then,

$$\begin{cases} z_{F_2} - z_{F_1} = 0 \\ \left(x_{U_3} - x_{U_2}\right)\left(x_{F_2} - x_{F_1}\right) + \left(y_{U_3} - y_{U_2}\right)\left(y_{F_2} - y_{F_1}\right) + \left(z_{U_3} - z_{U_2}\right)\left(z_{F_2} - z_{F_1}\right) = 0 \end{cases}. \tag{6}$$

https://doi.org/10.1017/S0263574718001406 Published online by Cambridge University Press

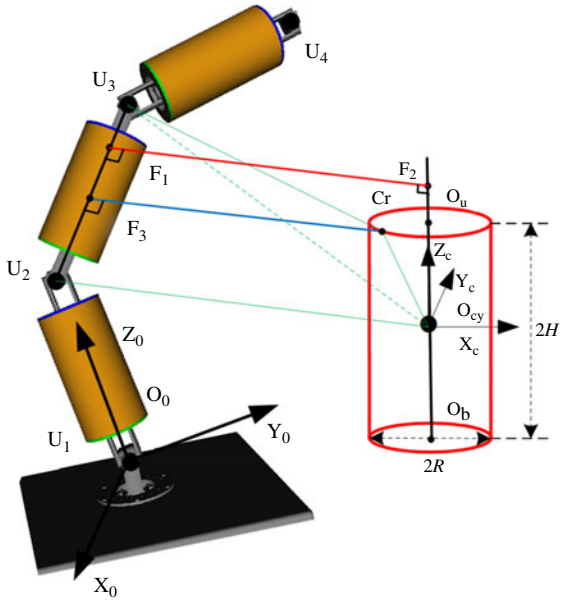


Fig. 9. One perpendicular foot on the link, the other outside the obstacle.

Points F_1 and F_2 are located on $\overrightarrow{U_2U_3}$ and $\overrightarrow{O_bO_u}$, respectively:

$$\frac{x_{F_1}-x_{U_2}}{x_{U_3}-x_{U_2}}=\frac{y_{F_1}-y_{U_2}}{y_{U_3}-y_{U_2}}=\frac{z_{F_1}-z_{U_2}}{z_{U_3}-z_{U_2}} \tag{7}$$

$$\begin{cases} x_{F_2}=0 \\ y_{F_2}=0 \\ z_{F_2}=z_{F_1} \end{cases}. \tag{8}$$

Simultaneous equations are listed as follows:

$$\begin{cases} x_{F_1}=\dfrac{\left(x_{U_3}-x_{U_2}\right)\left(-y_{U_2}y_{U_3}+y_{U_2}^2\right)+x_{U_2}\left(y_{U_3}-y_{U_2}\right)^2}{\left(x_{U_3}-x_{U_2}\right)^2+\left(y_{U_3}-y_{U_2}\right)^2} \\ y_{F_1}=\dfrac{\left(y_{U_3}-y_{U_2}\right)\left(-x_{U_2}x_{U_3}+x_{U_2}^2\right)+y_{U_2}\left(x_{U_3}-x_{U_2}\right)^2}{\left(x_{U_3}-x_{U_2}\right)^2+\left(y_{U_3}-y_{U_2}\right)^2} \\ z_{F_1}=\dfrac{\left(z_{U_3}-z_{U_2}\right)\left[-y_{U_2}\left(y_{U_3}-y_{U_2}\right)-x_{U_2}\left(x_{U_3}-x_{U_2}\right)\right]}{\left(x_{U_3}-x_{U_2}\right)^2+\left(y_{U_3}-y_{U_2}\right)^2}+z_{U_2} \end{cases}. \tag{9}$$

The minimum distance between the link and the cylinder is

$$d_{cy}=\sqrt{\left(x_{F_1}-x_{F_2}\right)^2+\left(y_{F_1}-y_{F_2}\right)^2+\left(z_{F_1}-z_{F_2}\right)^2}. \tag{10}$$

(2) Perpendicular distance 2

When one perpendicular foot falls on the current link and the other falls on the outside of the cylindrical obstacle, the minimum distance between the link and the obstacle is no longer the length of the perpendicular line F_1F_2, as shown in Fig. 9. Three points (i.e., U_2, U_3, and O_{cy}) can form a spatial plane, and this plane intersects with the upper surface of the cylinder obstacle at point Cr (Cr is the abbreviation of "cross point"). A perpendicular line is then drawn from point Cr to line U_2U_3, and the perpendicular foot is marked as F_3. The length of $|\overrightarrow{F_3Cr}|$ is defined as the minimum distance from the current link to the cylinder obstacle.

https://doi.org/10.1017/S0263574718001406 Published online by Cambridge University Press

The equation of the plane formed by U_2, U_3, and O_{cy} in space, the intersection of the plane equation, and the upper surface of the cylindrical obstacle are solved as follows.

1) The solution of the perpendicular plane equation and the perpendicular foot

The equation of cylindrical circle is

$$\begin{cases} \left(x - x_{O_u}\right)^2 + \left(y - y_{O_u}\right)^2 = R^2 \\ z = z_{O_u} \end{cases}. \tag{11}$$

The plane formed by three points $\left(O_{cy}\left(x_{O_{cy}}, y_{O_{cy}}, z_{O_{cy}}\right)\right.$, $U_2\left(x_{U_2}, y_{U_2}, z_{U_2}\right)$, and $U_3\left(x_{U_3}, y_{U_3}, z_{U_3}\right)\big)$ is

$$A_1 x + B_1 y + C_1 z + D_1 = 0 \tag{12}$$

where

$$\begin{cases} A_1 = y_{O_{cy}} z_{U_2} - y_{O_{cy}} z_{U_3} - z_{O_{cy}} y_{U_2} + z_{O_{cy}} y_{U_3} + y_{U_2} z_{U_3} - y_{U_3} z_{U_2} \\ B_1 = -x_{O_{cy}} z_{U_2} + x_{O_{cy}} z_{U_3} + z_{O_{cy}} x_{U_2} - z_{O_{cy}} x_{U_3} - x_{U_2} z_{U_3} + x_{U_3} z_{U_2} \\ C_1 = x_{O_{cy}} y_{U_2} - x_{O_{cy}} y_{U_3} - y_{O_{cy}} x_{U_2} + y_{O_{cy}} x_{U_3} + x_{U_2} y_{U_3} - x_{U_3} y_{U_2} \\ D_1 = -x_{O_{cy}} y_{U_2} z_{U_3} + x_{O_{cy}} y_{U_3} z_{U_2} + x_{U_2} y_{O_{cy}} z_{U_3} - x_{U_3} y_{O_{cy}} z_{U_2} - x_{U_2} y_{U_3} z_{O_{cy}} + x_{U_3} y_{U_2} z_{O_{cy}} \end{cases}. \tag{13}$$

The coordinate of point Cr can be obtained as follows:

$$\begin{cases} x_{Cr} = \dfrac{-B \pm \sqrt{B^2 - 4AC}}{2A} \\ y_{Cr} = E_1 x_{Cr} + F_1 \\ z_{Cr} = z_{O_u} \end{cases} \tag{14}$$

where $A = (E_1 + 1)$, $B = 2\left(E_1 F_1 - E_1 y_{U_2} - x_{U_2}\right)$, $C = x_{U_2}^2 + \left(F_1 - y_{U_2}\right)^2 - R^2 E_1 = -\frac{A_1}{B_1}$, and $F_1 = \frac{C_1 z_{U_2} + D_1}{B_1}$.

2) The solution of perpendicular foot F_3

The linear equation of U_2U_3 can be expressed as follows:

$$\frac{x - x_{U_2}}{x_{U_3} - x_{U_2}} = \frac{y - y_{U_2}}{y_{U_3} - y_{U_2}} = \frac{z - z_{U_2}}{z_{U_3} - z_{U_2}}. \tag{15}$$

The coordinate of F_3 can be obtained as follows:

$$\begin{cases} x_{F_3} = x_{U_2} + \dfrac{(x_{U_3} - x_{U_2})\left((x_{U_3} - x_{U_2})(x_{Cr} - x_{U_2}) + (y_{U_3} - y_{U_2})(y_{Cr} - y_{U_2}) + (z_{U_3} - z_{U_2})(z_{Cr} - z_{U_2})\right)}{(x_{U_3} - x_{U_2})^2 + (y_{U_3} - y_{U_2})^2 + (z_{U_3} - z_{U_2})^2} \\ y_{F_3} = y_{U_2} + \dfrac{(y_{U_3} - y_{U_2})\left((x_{U_3} - x_{U_2})(x_{Cr} - x_{U_2}) + (y_{U_3} - y_{U_2})(y_{Cr} - y_{U_2}) + (z_{U_3} - z_{U_2})(z_{Cr} - z_{U_2})\right)}{(x_{U_3} - x_{U_2})^2 + (y_{U_3} - y_{U_2})^2 + (z_{U_3} - z_{U_2})^2} \\ z_{F_3} = z_{U_2} + \dfrac{(z_{U_3} - z_{U_2})\left((x_{U_3} - x_{U_2})(x_{Cr} - x_{U_2}) + (y_{U_3} - y_{U_2})(y_{Cr} - y_{U_2}) + (z_{U_3} - z_{U_2})(z_{Cr} - z_{U_2})\right)}{(x_{U_3} - x_{U_2})^2 + (y_{U_3} - y_{U_2})^2 + (z_{U_3} - z_{U_2})^2} \end{cases}. \tag{16}$$

The minimum distance between the current link and the cylinder is

$$d_{Cr} = \sqrt{\left(x_{Cr} - x_{F_3}\right)^2 + \left(y_{Cr} - y_{F_3}\right)^2 + \left(z_{Cr} - z_{F_3}\right)^2}. \tag{17}$$

3) Perpendicular distance 3

When one perpendicular foot is located outside of the link and the other perpendicular foot is located inside the obstacle, the minimum distance between the link and the obstacle is no longer the length of the perpendicular line of F_1F_2, which is shown in Fig. 10. It becomes the distance from the point U_2 or U_3 to the obstacle, that is, $|\overrightarrow{U_2F_3}|$.

https://doi.org/10.1017/S0263574718001406 Published online by Cambridge University Press

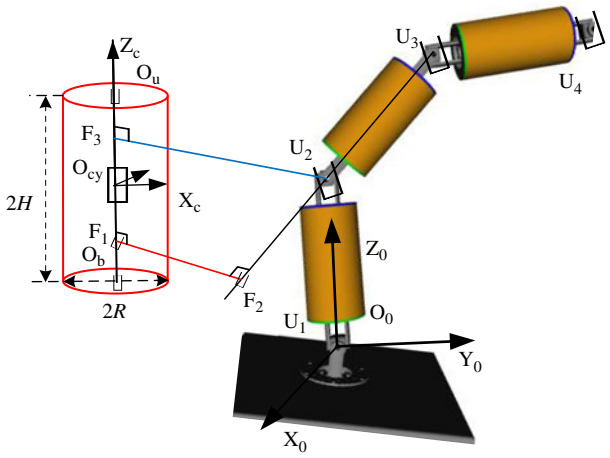


Fig. 10. One perpendicular foot outside the link and the other inside the obstacle.

The calculation method is similar to that of perpendicular distance 2 described previously, and the minimum distance is calculated as follows:

$$d_{cy} = \sqrt{\left(x_{F_3} - x_{U_2}\right)^2 + \left(y_{F_3} - y_{U_2}\right)^2 + \left(z_{F_3} - z_{U_2}\right)^2}. \tag{18}$$

The model described using the practical geometry function can be built similar to the actual obstacle, and it is also defined as the dangerous boundary. The accuracy of the quantitative criterion is then ensured.

4. Obstacle-Avoiding Trajectory Planning Using the Modified Modal Function

Based on the hybrid obstacle models, a modified fitting method[28] for the backbone curve can be used to complete the hybrid obstacle-avoidance task. To realize the local obstacle avoidance of the hyper-redundant manipulator, the proposed configuration parameters (i.e., the arm angle and the equivalent link) are adjusted in this paper. These parameters fully excavate the redundant capability of the hyper-redundant manipulator.

4.1. Modified fitting method for backbone curve

In the modified fitting method, the straight line between two adjacent odd-numbered universal joints (i.e., U_{2i-1}, U_{2i+1}) is defined as the equivalent link; its length is ρ_i, and the angle between $\overrightarrow{O_i\tilde{U}^a_{2i}}$ and $\overrightarrow{O_iU^{\psi}_{2i}}$ is defined as ψ_i[4]. The concept is shown in Fig. 11. In the local self-motion space, the spatial position of the universal joint can be controlled by adjusting the arm angle. By controlling the length of the equivalent link, the potential position of the universal joint on the backbone can be fully used. Although the overall configuration of the hyper-redundant manipulator is still determined by the backbone, the hyper-redundant manipulator works more flexibly due to the introduction of configuration parameters.

As the configuration of the manipulator is no longer completely limited by the backbone, the obstacle-avoidance application in a dynamic environment can be easily realized by adjusting the configuration parameters instead of re-determining the backbone curve. From this viewpoint, the traditional method[29] is actually a special case of the modified modal method.

For dealing with obstacle-avoidance problems, the modified method makes the following two improvements.

1) The equivalent link length between two adjacent odd joints ρ_i is parameterized. As the position of each odd universal joint moves along the backbone by adjusting the equivalent link parameter, the equivalent link length can optimize the obstacle-avoidance problem.

https://doi.org/10.1017/S0263574718001406 Published online by Cambridge University Press

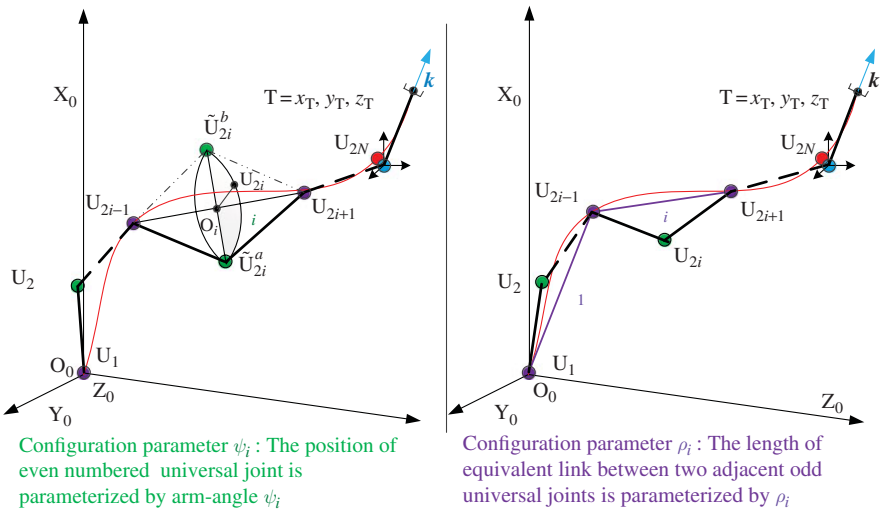


Fig. 11. Concept of the obstacle-avoidance configuration parameters.

2) The position of each even-numbered universal joint is parameterized by arm angle ψ_i. Hence, the even-numbered universal joints no longer have to be located on the backbone. The local obstacle-avoidance problem can also be optimized by the arm angle.

4.2. Single configuration parameter adjusting for obstacle avoidance

According to Fig. 11, the modified modal method can be summarized as follows. First, the universal joint U_{2N} can be determined by matching the direction vector of end-effector k. Second, the rest of the even- and odd-numbered universal joints are optimized by adjusting the configuration parameters (i.e., the equivalent link length and the arm angle). As this paper focuses on the relationship between the configuration parameters and the configuration of the manipulator, the effectiveness of the equivalent link length and the arm angle is analyzed. The configuration parameters can be adjusted to change the position of the universal joint. As such, the distances between the manipulator and the obstacles are kept within a reasonable range.

4.2.1. Adjustment of equivalent link parameter. Based on the backbone of the modal function, the configurations figure is presented in Fig. 12, and the obstacle-avoidance figure is presented in Fig. 13. Both rely on equivalent length.

U_i^{ρ}——the position of the universal joint based on the length of the equivalent link
F_i——the perpendicular foot of the perpendicular line
F_i^{ρ}——the perpendicular foot based on the length of the equivalent link

The length of the equivalent link is the independent variable. Actual links are represented by $U_{2i-1}U_{2i}^{\rho_i^b}$, $U_{2i}^{\rho_i^b}U_{2i+1}$; equivalent links are represented by $U_{2i-1}U_{2i+1}^{\rho}$, and the reference plane is represented by the dotted and solid lines (i.e., $U_{2i-1}U_{2i+1}^{\rho}U_{2N}$). To achieve obstacle avoidance, it is necessary to iteratively solve the reasonable length of the equivalent link.

According to Fig. 13, the minimum distance between the manipulator and the obstacle can be calculated by the method in Section 3.2. To meet the obstacle-avoidance requirement, it is necessary to optimize the length of the equivalent link (i.e., ρ_i).

4.2.2. Adjustment of arm-angle parameter. Once the length of the equivalent link is determined (i.e., $\rho_i = 1.8L$), the arm angle ψ_i becomes the only parameter to affect joint angles. The position of the end-effector and the universal joint (i.e., U_{2i+1}) are listed in Eqs. (19) and (20), respectively.

https://doi.org/10.1017/S0263574718001406 Published online by Cambridge University Press

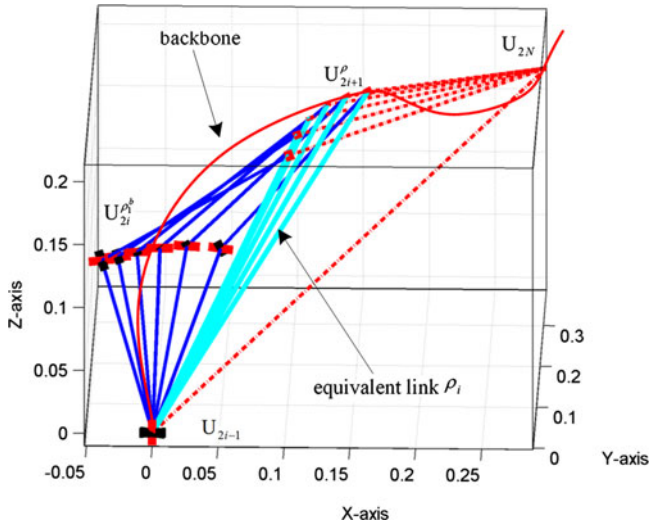


Fig. 12. Configurations relying on equivalent length.

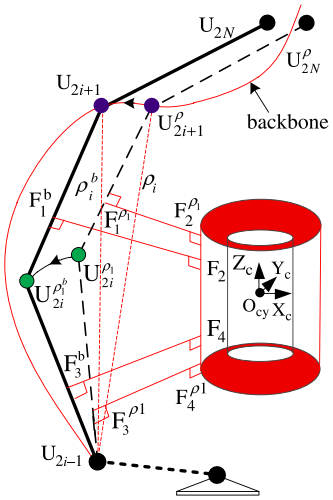


Fig. 13. Obstacle avoidance relying on equivalent length ρ_i.

The corresponding configuration is drawn in Fig. 14. The obstacle-avoidance figure is presented in Fig. 15, and it relies on the arm angle.

$$T_0 = \left[x_{T_0}, y_{T_0}, z_{T_0}\right] = [0.3000\text{m}, 0.5000\text{m}, 0.4000\text{m}] \tag{19}$$

$$U_{2i+1} = [0.1315\text{m}, 0.1699\text{m}, 0.2086\text{m}] \tag{20}$$

U^{ψ}_{i} ——the position of the universal joint based on arm angle ψ
$\triangle U_{2i-1}U_{2i+1}U_{2N}$——the reference plane of arm angle ψ_i
F^{ψ}_{i} ——the perpendicular foot based on arm angle ψ_i

As Fig. 14 shows, when the arm angle varies in the interval $\psi_i = [0, \pi]$ (when the arm angle meets $\psi_i = [\pi, 2\pi]$, the two links form the other half-symmetrical configuration, which is not repeated here), a series of corresponding configurations can be obtained.

If the obstacle must be avoided, the arm angle should be adjusted according to the minimum distance, as shown in Fig. 15. The minimum distance can be calculated between the manipulator

https://doi.org/10.1017/S0263574718001406 Published online by Cambridge University Press

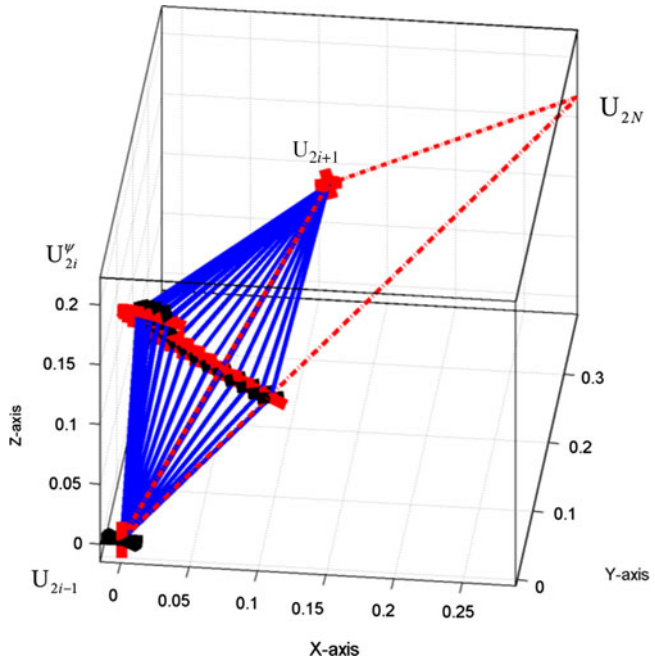


Fig. 14. Configuration in $\psi = [0, \pi]$.

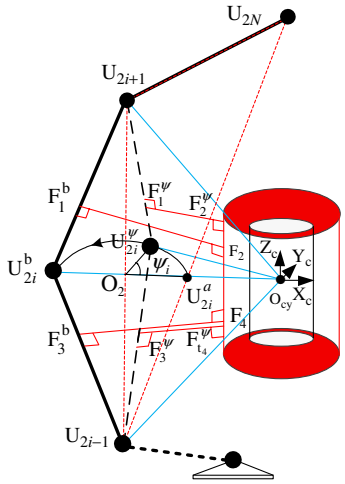


Fig. 15. Obstacle avoidance relying on arm angle ψ.

and the obstacle using the method in Section 3.2. To move the manipulator safely, it is necessary to optimize the arm angle (i.e., ψ_i) to ensure that the distance between the obstacle and the manipulator $\left(\text{i.e., } \left|F_1^{\psi} F_2^{\psi}\right|\right)$ meets the requirements of obstacle avoidance.

4.3. Configuration adjustment for the avoidance of obstacle, singularity, and joint limit

It can be seen from the paper that the avoidance of obstacle is taken as the example to introduce the adjustment of the equivalent link and the arm angle. In fact, by adjusting the equivalent link and the arm angle, the configuration of the manipulator can be adjusted iteratively, thereby achieving the goals of the avoidance of obstacle, singularity, and joint limit. The possible modes of the adjustment are summarized as follows:

Mode 1: The avoidance of obstacle, singularity, and joint limit is simultaneously achieved only by adjusting the length of equivalent link ρ_i.

Mode 2: The avoidance of obstacle, singularity, and joint limit is simultaneously achieved only by changing the value of arm angle ψ_i.

https://doi.org/10.1017/S0263574718001406 Published online by Cambridge University Press

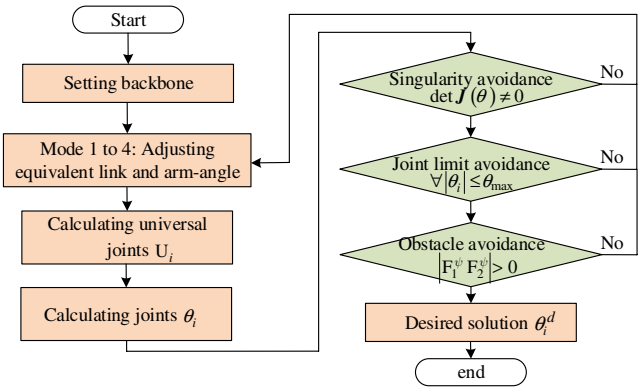


Fig. 16. Configuration adjustment for the avoidance of obstacle, singularity, and joint limit.

Mode 3: The avoidance of obstacle, singularity, and joint limit is simultaneously achieved by adjusting equivalent link ρ_i and arm angle ψ_i cooperatively.

Mode 4: The avoidance of obstacle, singularity, and joint limit is simultaneously achieved by using the adjacent group of configuration parameters (i.e., ψ_i, ρ_i, ψ_{i+1}, ρ_{i+1}) synergistically.

Based on the above introduction, the configuration adjustment for the avoidance of obstacle, singularity, and joint limit is described in Fig. 16. The criterion for the avoidance of singularity is $\det J(\theta) \neq 0$, and $J(\theta)$ is defined as the Shape Jacobian;[30] the criterion for the avoidance of joint limit is $\forall |\theta_i| \leq \theta_{\max}$, and θ_i is defined as the solved joint angle in the iteration process, and $\theta_{\max}$ is the joint limit; the criterion for the avoidance of obstacle is $\left|F_1^{\psi} F_2^{\psi}\right| > 0$, and $\left|F_1^{\psi} F_2^{\psi}\right|$ is defined as the minimum distance between the obstacle and the manipulator.

5. Case Study

To verify the avoidance capability of obstacle, singularity, and joint limit for the proposed method, the hyper-redundant manipulator is set to work in a confined environment with different obstacles. The hyper-redundant manipulator is simplified as segments, and the obstacles are simplified as cylinders, cuboid, cones, etc. Based on the proposed hybrid models, the pseudo-distance and the Euclidean distance are calculated as the obstacle-avoidance criteria. The obstacle avoidance of the hyper-redundant manipulator is achieved using the modified modal method. The redundant DOFs of the manipulator are converted into controllable parameters. As such, the flexibility of the hyper-redundant manipulator is fully exerted.

When the coordinates of start point A (x_a, y_a, z_a), the coordinates of end point C (x_c, y_c, z_c), and times of interpolation N are given, the interpolation step can be expressed as follows:

$$\begin{cases} \Delta x = (x_c - x_a)/(N+1) \\ \Delta y = (y_c - y_a)/(N+1) \\ \Delta z = (z_c - z_a)/(N+1) \end{cases}. \tag{21}$$

Any point i $(1 \leq i \leq N)$ on the line can be represented as:

$$\begin{cases} x_i = x_a + \Delta x \cdot i \\ y_i = y_a + \Delta y \cdot i \\ z_i = z_a + \Delta z \cdot i \end{cases}. \tag{22}$$

The initial and finish positions are shown in Eqs. (23) and (24), respectively:

$$\begin{cases} \left[x_{T0}, y_{T0}, z_{T0}\right]^{\mathrm{T}} = [0.35\mathrm{m}, 0.30\mathrm{m}, 0.40\mathrm{m}]^{\mathrm{T}} \\ k_1 = [0.18, 0.91, 0.35]^{\mathrm{T}} \\ t_1 = 0\mathrm{s} \end{cases} \tag{23}$$

https://doi.org/10.1017/S0263574718001406 Published online by Cambridge University Press

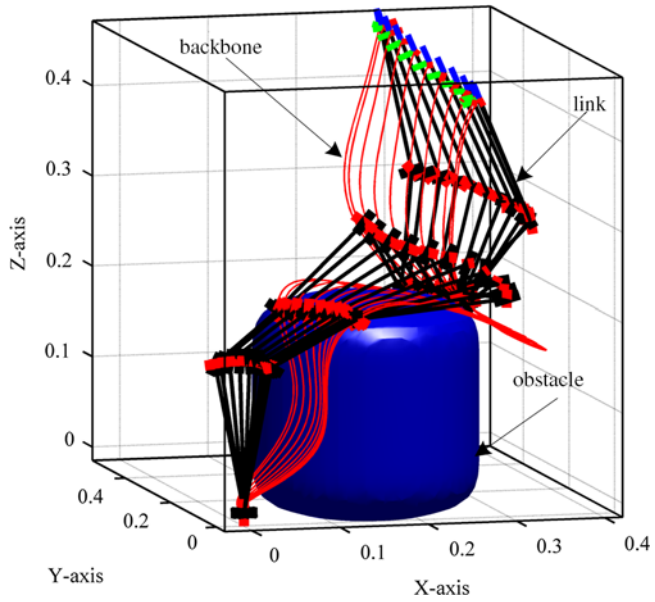


Fig. 17. Hyper-redundant manipulator, backbone, and obstacle.

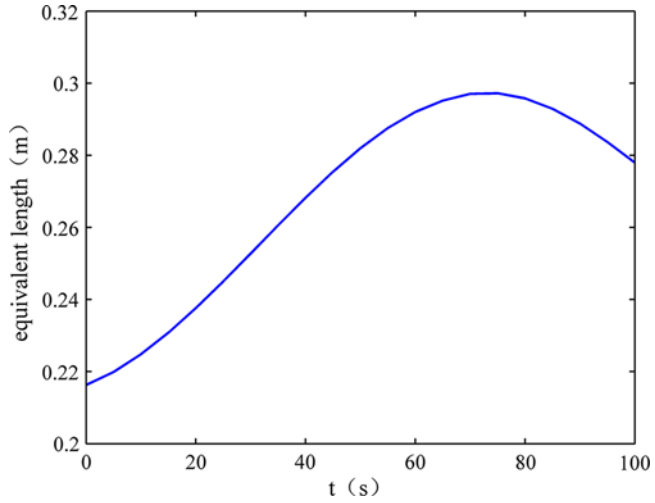


Fig. 18. Change of equivalent length of U_3U_5.

$$\begin{cases} [x_{\mathrm{Tf}}, y_{\mathrm{Tf}}, z_{\mathrm{Tf}}]^{\mathrm{T}} = [0.35\mathrm{m}, 0.55\mathrm{m}, 0.45\mathrm{m}]^{\mathrm{T}} \\ k_{\mathrm{f}} = [0.39, 0.70, 0.59]^{\mathrm{T}} \\ t_{\mathrm{f}} = 100\mathrm{s} \end{cases} . \tag{24}$$

5.1. Case 1: obstacle avoidance by adjusting the equivalent link

The initial and termination conditions are the same as in Case 1. For comparison, a third-order polynomial function is used to plan the motion trajectory between t_0 and t_{f}. Mode 1 in Section 4.3 is chosen to avoid the cylinder obstacle. The planned configuration, changes in equivalent link, angular velocity, and minimum distances to the cylinder obstacle are shown in Figs. 17–20, respectively.

5.2. Case 2: multiple obstacles avoidance by adjusting the arm angle

The initial and termination conditions are the same as above. The motion trajectory between t_0 and t_{f} is also planned by a third-order polynomial function. Mode 3 in Section 4.3 is chosen to avoid the obstacles (i.e., cylinder, cuboid, and cone). The configuration and the changes in arm angle,

https://doi.org/10.1017/S0263574718001406 Published online by Cambridge University Press

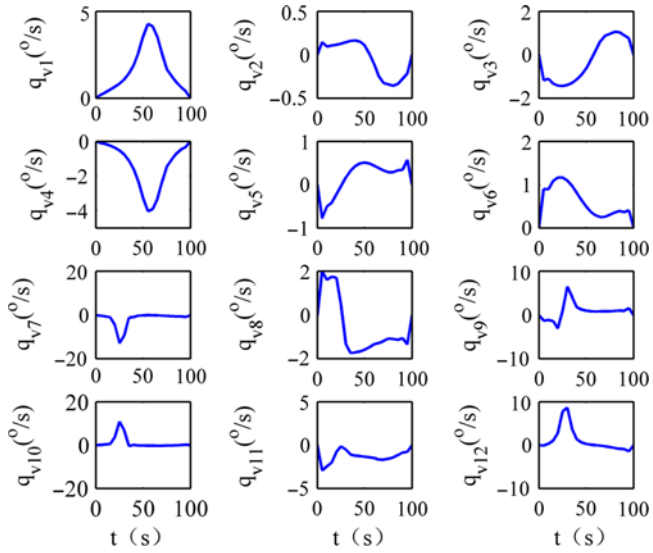


Fig. 19. Velocity of joints.

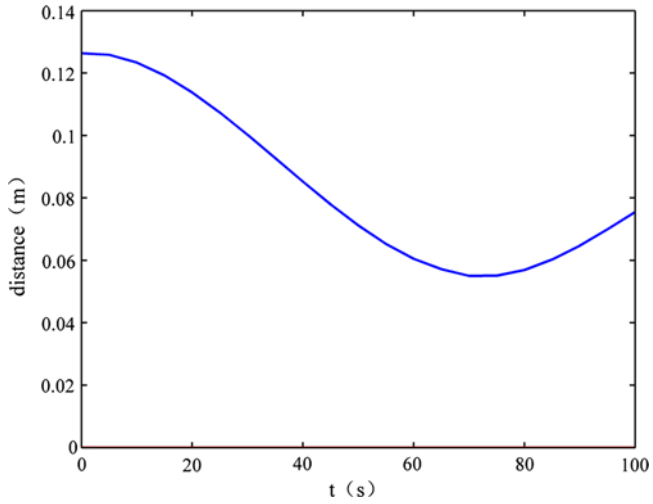


Fig. 20. Minimum distance.

angular velocity, and minimum distances to each obstacle are shown in Figs. 21–24, respectively. The pseudo-distance calculated by the model described using the super-quadric function and the Euclidean distance calculated by the model described using the practical geometry function are of different orders of magnitude. To facilitate the representation in this simulation, when the pseudo-distance value is greater than 0.25 m, the value is set to 0.25 m. In Fig. 24, the terms "cylinder," "cuboid," "cone," "Euclidean distance," and "pseudo-distance" are abbreviated as "Cy," "Cu," "Co," "Eu Dis," and "Ps Dis," respectively.

5.3. Case 3: experiment of confined truss crossing

5.3.1. Experiment setup.

(1) Experiment principle: First, the trajectory planning algorithm proposed in this paper is used to plan the desired trajectory of the hyper-redundant manipulator, and then, the hyper-redundant manipulator is controlled to repeat the desired trajectory. Before the experiment, the end position of the hyper-redundant manipulator is calibrated by using a laser tracking measurement system. In the experiment, the errors between the actual angles of the joints measured by the rotary encoders and the desired angles of the joints calculated by kinematics are both input into the

https://doi.org/10.1017/S0263574718001406 Published online by Cambridge University Press

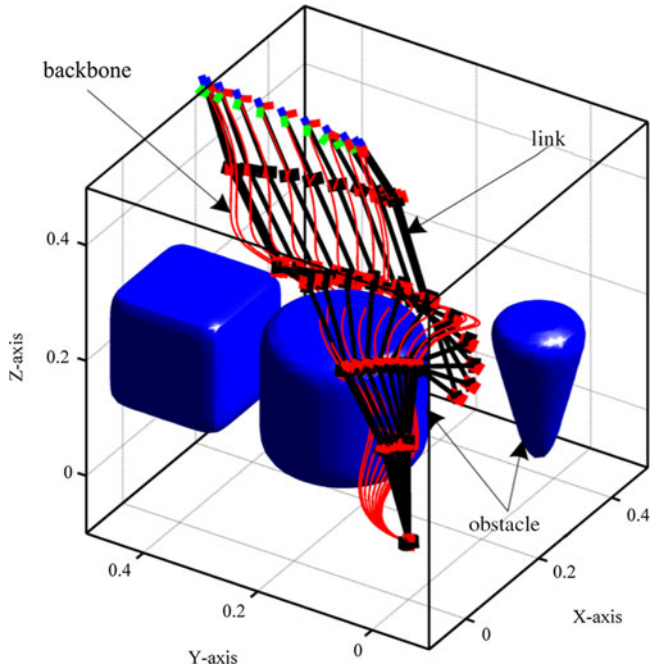


Fig. 21. Hyper-redundant manipulator, backbone, and obstacles.

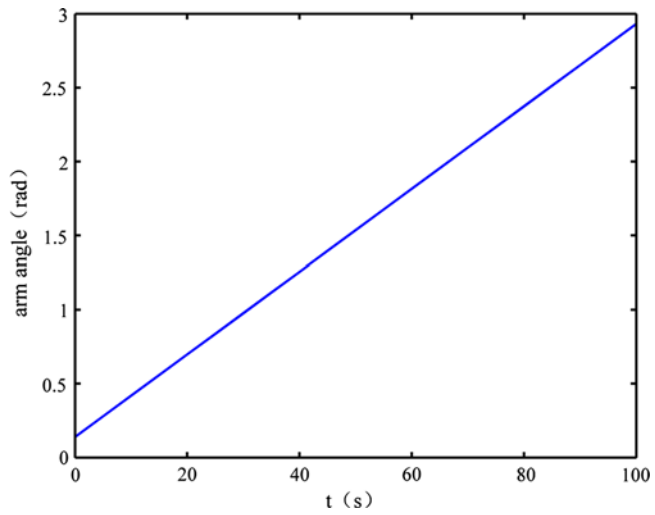


Fig. 22. Change in arm angle ψ_2.

proportional differential controller, so the higher control precision can be obtained by superimposing the dynamic feedforward compensation term. The data of the experiment are processed to verify the correctness of the trajectory planning method and the effectiveness of the dynamic control method for hyper-redundant manipulator.

(2) Experiment equipment: Laser tracker system, rotary encoder, cable pretension device, WIFI camera, vernier caliper, and a cable-driven hyper-redundant manipulator with 18 DOFs.

(3) Measurement method: The laser tracker system is used to calibrate the key positions of the hyper-redundant manipulator, and its accuracy is $10\mu m \pm 2.5\mu m/m$. The rotary encoder is used to measure the actual change of the cable's length, which is regarded as the feedback value of the closed-loop control, and its accuracy is 0.08°. A cable pretension device is used to ensure a reasonable preload of the cable, and the preload is set to 175 N based on the empirical value. The WIFI camera can transmit the target environment information to the host computer for the operator to control.

https://doi.org/10.1017/S0263574718001406 Published online by Cambridge University Press

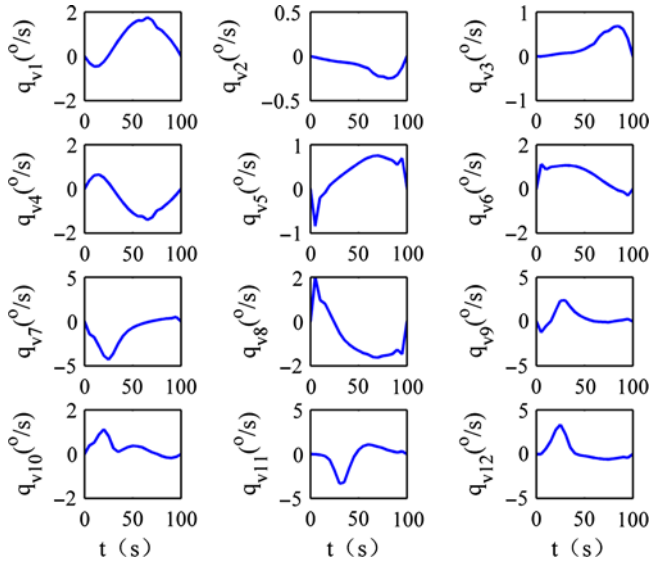


Fig. 23. Velocity of joints.

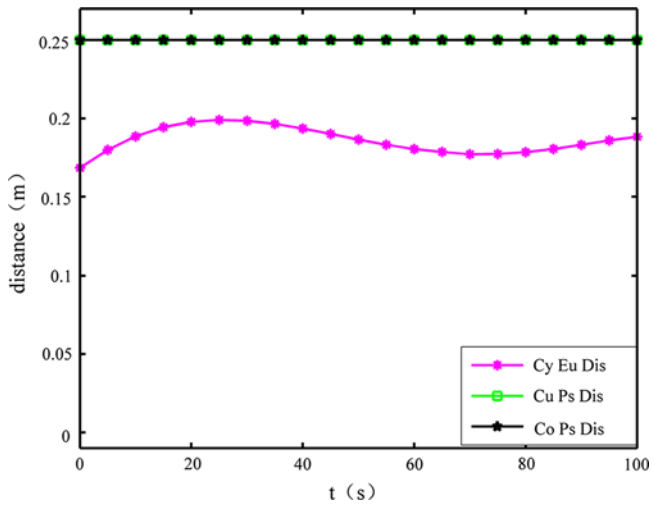


Fig. 24. Minimum distance.

(4) Experiment process: In order to verify the adaptability of the proposed method, it is necessary to carry out the confined space operation experiment for the hyper-redundant manipulator. The manipulator is supposed to inspect a truss structure. 25 mm aluminum tubes are used to build a tripod, and two sets of horizontal support tubes divided the tripod into a truss-like structure. The initial to final poses are set as (25)–(27). Then, the proposed methods are used to generate the trajectory of the manipulator. The desired joint angles are shown in Fig. 25.

$$T_s = \begin{bmatrix} 1 & 0 & 0 & 1332.00\text{mm} \\ 0 & 0 & -1 & 0 \\ 0 & 1 & 0 & 0 \\ 0 & 0 & 0 & 1 \end{bmatrix} \tag{25}$$

$$T_m = \begin{bmatrix} 0.0577 & -0.0002 & 0.9983 & 803.18\text{ mm} \\ 0.9983 & 0.0040 & -0.0577 & 135.27\text{ mm} \\ -0.0040 & 0.9990 & 0.0004 & -0.52\text{ mm} \\ 0 & 0 & 0 & 1 \end{bmatrix} \tag{26}$$

https://doi.org/10.1017/S0263574718001406 Published online by Cambridge University Press

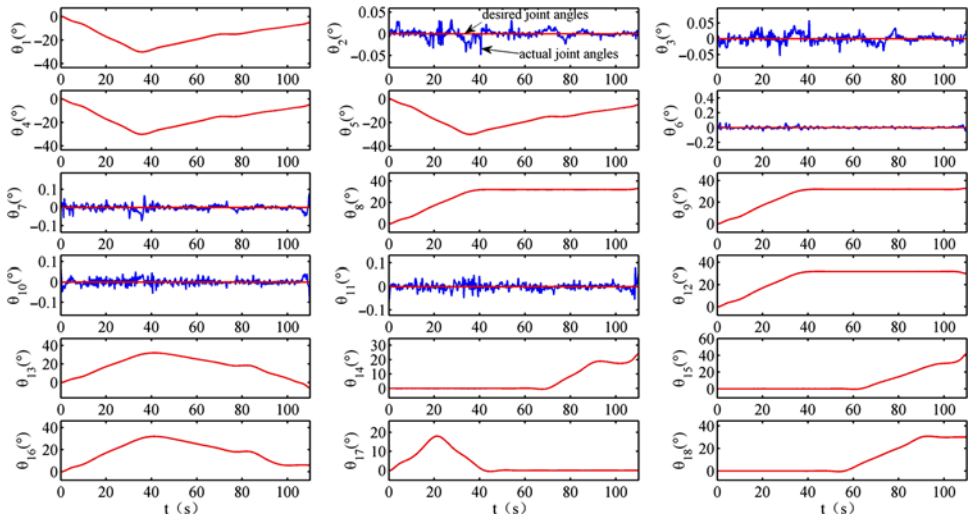


Fig. 25. Desired joint angles and actual joint angles.

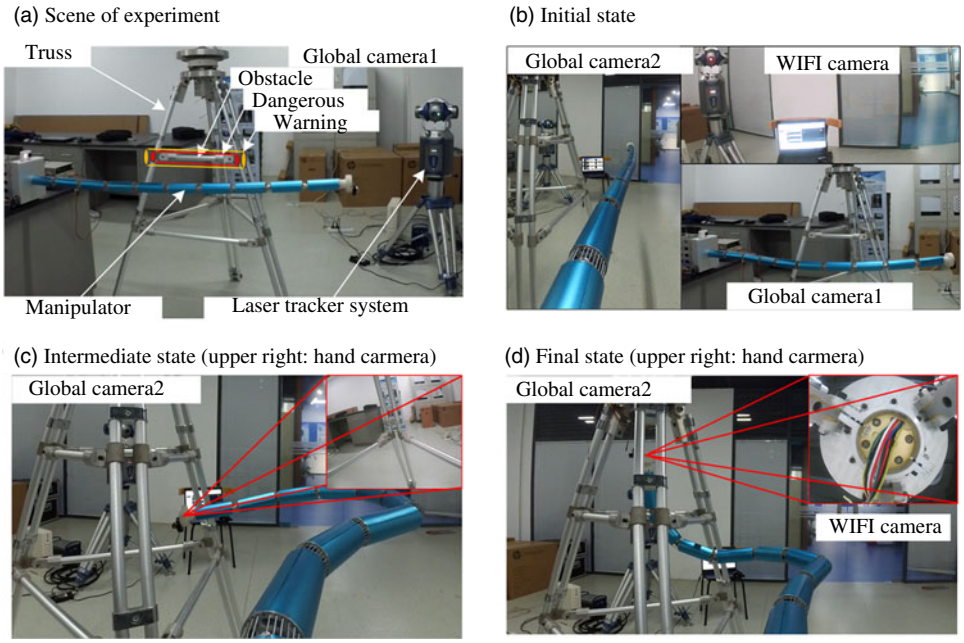


Fig. 26. Experiment process of confined truss crossing. (a) Scene of experiment; (b) Initial state; (c) Intermediate state; and (d) Final state.

$$T_f = \begin{bmatrix} -0.1142 & -0.2067 & 0.9717 & 712.29\,\text{mm} \\ -0.0766 & -0.9733 & -0.2160 & 410.82\,\text{mm} \\ 0.9904 & -0.0991 & 0.0953 & 340.93\,\text{mm} \\ 0 & 0 & 0 & 1 \end{bmatrix} \tag{27}$$

5.3.2. Experiment results. The movement of the manipulator is controlled to move with the desired joint angles of the manipulator at each step. The actual joint angles are also shown in Fig. 25. The results show that the proposed algorithm can meet the control requirements of the hyper-redundant manipulator. It also reflects the extremely confined space crossing capability of the hyper-redundant manipulator. The experiment process of confined truss crossing is shown in Fig. 26.

The experiment results show that the hyper-redundant manipulator has the ability to avoid obstacles in a confined environment with a desired control accuracy (no more than $\pm 0.05°$). However, there are still some control errors in the joint angles due to the influence of geometric parameter

https://doi.org/10.1017/S0263574718001406 Published online by Cambridge University Press

errors (mainly processing and assembly errors accounting for about 90% of the absolute position error of the manipulator). Combined with the characteristics of the hyper-redundant manipulator, the main sources of errors are summarized as follows: First, geometric parameters errors exist in hyper-redundant manipulator due to processing and assembly. Second, the cable has a certain elastic deformation error under the preload force. Third, there is a large sliding friction due to the relative motion between the cable and the cable hole, while the control model does not accurately consider this friction.

In order to improve the control precision of the cable-driven hyper-redundant manipulator, the following improvement strategies can be adopted. First, improve machining and assembly accuracy by calibrating geometric parameters and compensating for end positions in real time. Second, in order to improve the feedback control effect, higher precision detection components should be used. Thirdly, reduce the friction between the cable and the cable hole by using Teflon-coated material and modify the control model of the hyper-redundant manipulator by compensating friction and gravity terms.

6. Conclusion

This paper proposes a hybrid obstacle-avoidance method to realize on-orbit obstacle-avoidance planning for the hyper-redundant manipulator. The model described using the super-quadric function and the model described using the practical geometry function account for the efficiency and accuracy of the distance detection for a two-level protection strategy. In addition, the modified modal method considers the flexibility and solvability of the hyper-redundant manipulator. Based on the established hybrid models of the obstacle, it is possible to plan the trajectory in the safe area. When the manipulator works out of the warning boundary, the pseudo-distance can be used to determine the collision qualitatively. Furthermore, when the manipulator approaches the dangerous boundary, the Euclidean distance between the manipulator and the dangerous boundary can be accurately calculated to provide obstacle-avoidance criteria. As such, the main task of the hyper-redundant manipulator can be successfully completed by adjusting the configuration parameters in a narrow environment with multiple obstacles. To verify the avoidance capability of obstacle, singularity, and joint limit, two typical simulations of the 12-DOF manipulator and an experiment of 18-DOF manipulator are performed. The results show that the method is very efficient. While for a very cluttered environment, the dexterity of the hyper-redundant manipulator with 12 DOF and 18 DOF will be limited by the number of DOFs. By increasing the number of DOFs, the proposed method will also be effective for the hyper-redundant manipulator.

Acknowledgements

This work was supported by the National Natural Science Foundation of China (Grant No. 61573116, U1613227), Shenzhen Key Lab Fund of Mechanisms and Control in Aerospace (Grant No. ZDSYS201703031002066), the National Postdoctoral Program for Innovative Talents (Grant No. BX20180089), and China Postdoctoral Science Foundation (Grant No. 2018M641817).

References

1. P. Huang, F. Zhang, Z. Meng and Z. Liu, "Adaptive control for space debris removal with uncertain kinematics, dynamics and states," *Acta Astronaut.* 128, 416–430 (2016).
2. P. Huang, B. Liu and F. Zhang, "Configuration maintaining control of three-body ring tethered system based on thrust compensation," *Acta Astronaut.* 123, 37–50 (2016).
3. A. Flores-Abad, O. Ma, K. Pham and S. Ulrich, "A review of space robotics technologies for on-orbit servicing," *Prog. Aerosp. Sci.* 68, 1–26 (2014).
4. W. Xu, L. Yan, Z. Mu and Z. Wang, "Dual arm-angle parameterisation and its applications for analytical inverse kinematics of redundant manipulators," *Robotica* 34, 2669–2688 (2016).
5. R. Colbaugh, H. Seraji and K. L. Glass, "Obstacle avoidance for redundant robots using configuration control," *J. Rob. Syst.* **6**(6), 721–744 (1989).
6. N. Rahmanian-Shahri and I. Troch, "Collision-avoidance control for redundant articulated robots," *Robotica* **13**(02), 159–168 (1995).
7. V. Perdereau, C. Passi and M. Drouin, "Real-time control of redundant robotic manipulators for mobile obstacle avoidance," *Rob. Auton. Syst.* **41**(1), 41–59 (2002).
8. S. Bonner and R. B. Kelley, "A novel representation for planning 3-D collision-free paths," *IEEE Trans. Syst. Man Cybern.* **20**(6), 1337–1351 (1990).
9. S. I. Choi and B. K. Kim, "Obstacle avoidance control for redundant manipulators using collidability measure," *Robotica* **18**(02), 143–151 (2000).

https://doi.org/10.1017/S0263574718001406 Published online by Cambridge University Press

10. K. S. Hwang and M. Y. Ju, "3D collision-free motion based on collision index," *J. Intell. Rob. Syst.* **33**(1), 45–60 (2002).
11. R. V. Patel, F. Shadpey, F. Ranjbaran and J. Angeles, "A collision-avoidance scheme for redundant manipulators: theory and experiments," *J. Rob. Syst.* **22**(12), 737–757 (2005).
12. R. Volpe and P. Khosla, "Manipulator control with superquadric artificial potential functions: theory and experiments," *IEEE Trans. Syst. Man Cybern.* **20**(6), 1423–1436 (1990).
13. J. Kim and P. K. Khosla, "Real-time obstacle avoidance using harmonic potential functions," *IEEE Trans. Rob. Autom.* **8**(3), 338–349 (1992).
14. Z. Mu, Y. Yang, W. Xu, X. Gao and L. Xue, "Collision-free trajectory planning of redundant space manipulators based on pseudo-distance," Proceeding of the 11th World Congress on Intelligent Control and Automation, Shenyang, China (2014) pp. 5223–5228.
15. Z. Mu, W. Xu and B. Liang, "Avoidance of multiple moving obstacles during active debris removal using a redundant space manipulator," *Int. J. Cont. Autom. Syst.* **15**(2), 815–826 (2017).
16. K. Glass, R. Colbaugh, D. Lim and H. Seraji, "Real-time collision avoidance for redundant manipulators," *IEEE Trans. Rob. Autom.* **11**(3), 448–457 (1995).
17. E. Yoshida, C. Esteves, I. Belousov, J. P. Laumond, T. Sakaguchi and K. Yokoi, "Planning 3-D collision-free dynamic robotic motion through iterative reshaping," *IEEE Trans. Rob.* **24**(5), 1186–1198 (2008).
18. E. Freund, M. Schluse and J. Rossmann, "Dynamic collision avoidance for redundant multi-robot systems," Proceedings of IEEE/RSJ International Conference on Intelligent Robots and Systems, Maui, HI (2001) pp. 1201–1206.
19. R. V. Mayorga, "An appropriate bounded method for the on-line obstacle avoidance of redundant manipulators," Proceedings of IEEE/RSJ International Conference on Intelligent Robots and Systems, Grenoble, France (1997) pp. 1700–1705.
20. H. Seraji and B. Bon, "Real-time collision avoidance for position-controlled manipulators," *IEEE Trans. Rob. Autom.* **15**(4), 670–677 (1999).
21. W. Xu, J. Zhang, H. Qian and Y. Chen, "Identifying the singularity conditions of Canadarm2 based on elementary Jacobian transformation," IEEE/RSJ International Conference on Intelligent Robots and Systems, Tokyo, Japan (2013) pp. 795–800.
22. W. Xu, J. Zhang, B. Liang and B. Li, "Singularity analysis and avoidance for robot manipulators with nonspherical wrists," *IEEE Trans. Ind. Electron* **63**(1), 277–290 (2015).
23. S. Chiaverini, B. Siciliano and O. Egeland, "Review of damped least squares inverse kinematics with experiments on an industrial robot manipulator," *IEEE Trans. Contr. Syst. Technol.* **2**(2), 123–134 (1994).
24. A. Colomé and C. Torras, "Closed-loop inverse kinematics for redundant robots: comparative assessment and two enhancements," *IEEE/ASME Trans. Mech.* **20**(2), 944–955 (2015).
25. G. S. Chirikjian and J. W. Burdick, "A modal approach to hyper-redundant manipulator kinematics," *IEEE Trans. Rob. Autom.* **10**(3), 343–354 (1994).
26. G. S. Chirikjian and J. W. Burdick, "An obstacle avoidance algorithm for hyper-redundant manipulators," Proceedings of IEEE International Conference on Robotics and Automation, Cincinnati, OH (1990) pp. 625–631.
27. G. S. Chirikjian, Theory and applications of hyper-redundant robotic mechanisms. *Ph.D. Dissertation* (California Institute of Technology, 1992).
28. W. Xu, Z. Mu, T. Liu and B. Liang, "A modified modal method for solving the mission-oriented inverse kinematics of hyper-redundant space manipulators for on-orbit servicing," *Acta Astronaut.* 139, 54–66 (2017).
29. F. Fahimi, H. Ashrafiuon and C. Nataraj, "Obstacle avoidance for spatial hyper-redundant manipulators using harmonic potential functions and the mode shape technique," *J. Rob. Syst.* **20**(1), 23–33 (2003).
30. H. Mochiyama, and H. Kobayashi, "The shape Jacobian of a manipulator with hyper degrees of freedom," *IEEE International Conference on Robotics and Automation*, Detroit, Michigan (1999) pp. 2837–2842.

https://doi.org/10.1017/S0263574718001406 Published online by Cambridge University Press